

## Link between glacial striation morphology and induced drag

## Lucas K. Zoet<sup>†</sup>, Lillian Smith, Alex Mixtli, Jeremy Brooks, and Dougal D. Hansen

Department of Geoscience, University of Wisconsin-Madison, Madison, Wisconsin 53706, USA

#### ABSTRACT

Abrasion acts to smooth glacial terrains and leaves behind linear scratch-like features (striations) on bedrock landscapes. Striations are often used as measures of glacier flow directions, but their morphology can also provide information about the subglacial stress conditions that produced the features. While striations are often abundant in the field, the processes that create them can be opaque and hard to examine in situ because they occur under thick layers of flowing ice. To alleviate that difficulty and provide information for interpretation of the populations of striations that are observed in the field, we conducted a set of laboratory experiments in which a ring of temperate debris-laden ice was slid atop a planar marble bed under various contact force conditions that led to the creation of hundreds of striations. During the experiment, numerous glaciological properties were continuously measured, including the resistive drag. Following the completion of the experiments, the marble beds were extracted, and the striations were measured for length and categorized by morphological type, and a subset was measured using a highresolution white-light profilometer. These experiments showed that, similar to field observations, type 2 striations were initially the most abundant; however, we found that type 3 striations became the most abundant at large displacements. We found good correlation between the abundance of striations as a function of displacement and measured drag as a function of displacement. When taken together, these results suggest that, in natural settings, ice flow around small roughness elements in glacier beds can "reset" the basal debris field, causing striations to become more abundant in their wake. As roughness is linked to quarrying, abrasion rates may increase in areas of increased quarrying.

Lucas K. Zoet https://orcid.org/0000-0002 -9635-4051

†lzoet@wisc.edu

GSA Bulletin; published online 23 February 2024

#### 1. INTRODUCTION

Hard-bedded glacial terrains are sculpted by a combination of erosional processes: abrasion acting to smooth bedrock and quarrying acting to roughen the bed. Quarrying occurs as inhomogeneous stresses exerted by overriding ice extend bedrock fractures until bedrock blocks become isolated (Hallet, 1996; Iverson, 2012; Woodard et al., 2019). Those isolated blocks are then removed from the bed and entrained within the overriding ice, becoming tools that can be used for abrading the bed (Hallet, 1979, 1981). In contrast to quarrying, abrasion is the continual and gradual wearing away of the underlying bedrock. During abrasion, clasts embedded in the basal ice are pressed into and dragged atop the underlying bedrock by the overriding ice. As the clasts in contact with the bed are moved forward, indenting tips remove minuscule amounts of the underlying rock as well as material from the indenting clasts (Iverson, 1990, 1991; Hansen and Zoet, 2019). The friction between the clast and the bed also gives rise to a resistive drag that affects glacier sliding speed (Mathews, 1979; Hallet, 1981; Iverson et al., 2003, 2019; Cohen et al., 2005; Thompson et al., 2020). The material removed from the bed via abrasion results in the formation of linear scratch features, commonly called striations (Fig. 1A; Iverson, 1991; Benn and Evans, 2014). The amount of material removed in the striations depends on the hardness contrast between the indenter clast and the underlying bedrock, the rate of forward clast movement, the force with which the clast is pressed into the underlying bed (i.e., contact force), and the concentration of indenting clasts within the basal ice (Hallet, 1979, 1981; Hansen et al., 2023). The resultant striations record some combination of these abrading factors, but their morphology is often complex and difficult to interpret with respect to the factor(s) controlling abrasion.

Striations morphologies are often classified into three broad categories (Chamberlin, 1888; Iverson, 1991). Type 1 striations are "carrot-shaped" and start shallow but then deepen and widen as the indenter moves forward, before ter-

minating as the indenter is no longer pressed into the bed. Type 2 striations are more symmetric: They start shallow and narrow and then initially deepen and widen, followed by a general shallowing and narrowing as the indenter moves forward. Type 3 striations are also "carrot-shaped," but they start deep and wide and then shallow and narrow as they progress (Fig. 1B).

Clast-bed interactions not only produce a range of striation morphologies, but they also contribute to the amount of drag enacted on the overriding glacier (Zoet et al., 2013; Hansen and Zoet, 2019; Iverson et al., 2019; Thompson et al., 2020; Stevens et al., 2024). A clast lodged against the bed forces the ice to flow around, contributing to basal drag in much the same way as a bedrock obstacle. If the clast is only partially lodged, the force exerted by the ice moving around the clast is thus used in the formation of striations via the concentration of the clast force upon the clast's asperities (often called indenters), so, in this way, the striation records information about basal drag. The frictional drag between the clasts and the underlying bedrock increases the bulk drag resisting ice flow. This drag may be small in certain instances, especially when the underlying bedrock is planar (Thompson et al., 2020; Hansen et al., 2023), but it is likely greater when the underlying bedrock is adversely angled to the ice flow direction and has roughness elements over a range of sizes (Hallet, 1981; Iverson et al., 2019). Furthermore, the interactions of these clasts with the bed may regulate the transient frictional properties in such a manner that they set the local stability of subglacial slip, leading to certain patches of the bed generating seismic activity (Zoet et al., 2012, 2013, 2020).

The distribution of striation types and their general geomorphic form are of interest because they provide geologic evidence of the mechanical interactions between debris-rich ice and the underlying bed. For example, which type of striation is most prevalent for a specific site, and upon what does it depend? As certain types of striations come into and out of existence, does the bulk basal drag change in response? To address these types of questions and provide

https://doi.org/10.1130/B37351.1.

For permission to copy, contact editing@geosociety.org
© 2024 Geological Society of America



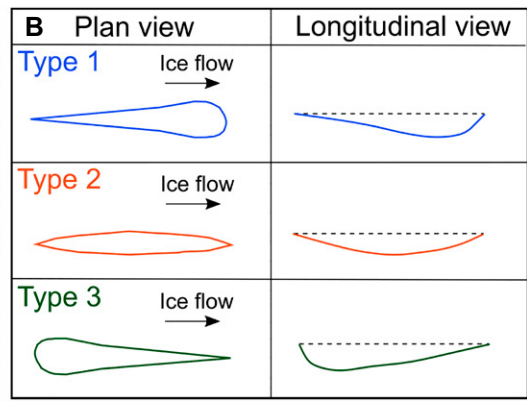


Figure 1. (A) Striation from Castleguard Glacier, Canada. Note the gloved finger for scale. (B) Schematic of the three different types of striations.

general samples of striation morphology, we conducted a pair of experiments using a novel cryogenic ring shear device in which temperate debris-laden ice was driven atop a planar marble bed under a constant slip speed while the resultant drag was measured. Following the completion of the experiments, hundreds of striations were measured for length, and their populations were categorized into type 1, 2, or 3. Finally, the morphology was measured for a subset of these striations using a white-light profilometer that was capable of sub-micron-resolution imaging. The results represent the range of striations that are possible under simple conditions (i.e., effective pressure, sliding velocity, bed composition, number of clasts, and basal melt rate were all effectively constant for the duration of the experiments).

## 2. STRIATION FORMATION

On the microscale, the morphology of striations is hypothesized to be linked to the angle at which the indenter intercepts the bed,  $\omega$  (Fig. 2; Gustafson et al., 1977; Iverson, 1991). If the indenter is angled near 45°, forward motion will cause the indenter to dig or plough into the surface, causing it to move deeper into the underlying rock as it progresses (i.e., type 1) due to the resulting pattern of tensile stresses induced in the rock (Iverson, 1991; Shah and Wong, 1997). This continues until the indenter either breaks, rotates out of this position, or becomes lodged against the bed. Conversely, indenters that are initially at an angle closer to 90° will initiate near their maximum depth and plough themselves out of the striation as they progress (i.e., type 3), essentially shallowing with further movement. Finally, type 2 striations are produced by clasts that plough themselves in, but then, as the indenter moves forward, small rotations cause the indenter angle to change, and the indenter slowly moves out of the striation. Therefore, striation morphology can be linked to clast indenter conditions and perhaps correlated with the subglacial forces required to rotate clasts and erode the bed material.

If the stress imparted by the indenter upon the rock causes a portion of the rock to exceed its yield strength, then an elastic fracture will form, and the indenter will move forward some small amount proportional to the fractured rock (Fig. 2; Engelder and Scholz, 1976; Scholz and Engelder, 1976; Scholz, 1987). For a clast moving in such a way where the forward motion is purely limited by this process, i.e., one that is effectively fully lodged against the bed, the rate of forward motion of the clast is regulated by the rate at which the underlying rock (or clast itself) fractures away. However, most clasts are not limited by a completely lodged scenario; instead, they are partially lodged and move forward at some rate that is closer to that of the ice speed, but in doing so, they still exert sufficient force on the underlying bedrock to fracture the bedrock (Thompson et al., 2020). In these cases, the

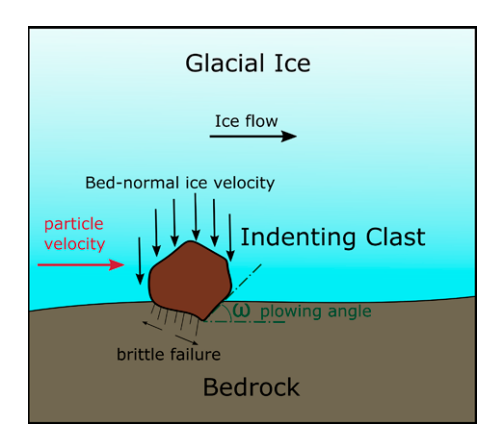


Figure 2. Schematic of an indenting clast. Ice flow is from left to right, and the bednormal ice flow velocity is regulating the contact force between the clast and bed. The indenter is angled at some degree,  $\omega$ , to the surface, and the stress placed upon the clast by the flowing ice is generating a tensile brittle failure in the lee of the clast.

resistance provided by the underlying material to the indenter is smaller than the force exerted by the ice pushing the clast forward, causing the indenter to travel at a speed near the actual ice speed (Hansen et al., 2023).

#### 3. METHODS

#### 3.1. Experimental Procedure

To assess the morphology of striations, we used a large-diameter cryogenic ring shear device that simulates in situ conditions at the base of glaciers (Zoet et al., 2023) to slide debris-laden temperate ice atop a rotationally fixed marble bed. Data gathered from a set of debris-laden ice flow experiments (for setup, see Hansen et al., 2023) were used to constrain the subglacial abrasion rule. The eroded volume created through subglacial abrasion was related to the precisely measured glaciological factors (e.g., sliding speed, overburden stress, water pressure, hardness contrast, basal melt rate, and vertical ice flow speed). In conducting the experiments, hundreds of striations were created and scanned to estimate the eroded volume. Then, we assessed the morphology and distributions of the striations in order to better understand the mechanics of abrasion and its link to striation morphology and basal drag. Detailed methods used to simulate the debris-laden subglacial slip have been previously reported in Hansen et al. (2023).

The University of Wisconsin–Madison cryogenic ring shear device (Fig. 3; Zoet et al., 2023) was used to slide debris-laden ice over a marble bed, producing striations (Fig. S1<sup>1</sup>). To induce the creation of striations, 309 clasts were positioned on the ring, and their placement

<sup>&</sup>lt;sup>1</sup>Supplemental Material. Document with images of all striation scans for reference and DEM data. Please visit https://doi.org/10.1130/GSAB.S.25008929 to access the supplemental material, and contact editing@geosociety.org with any questions.

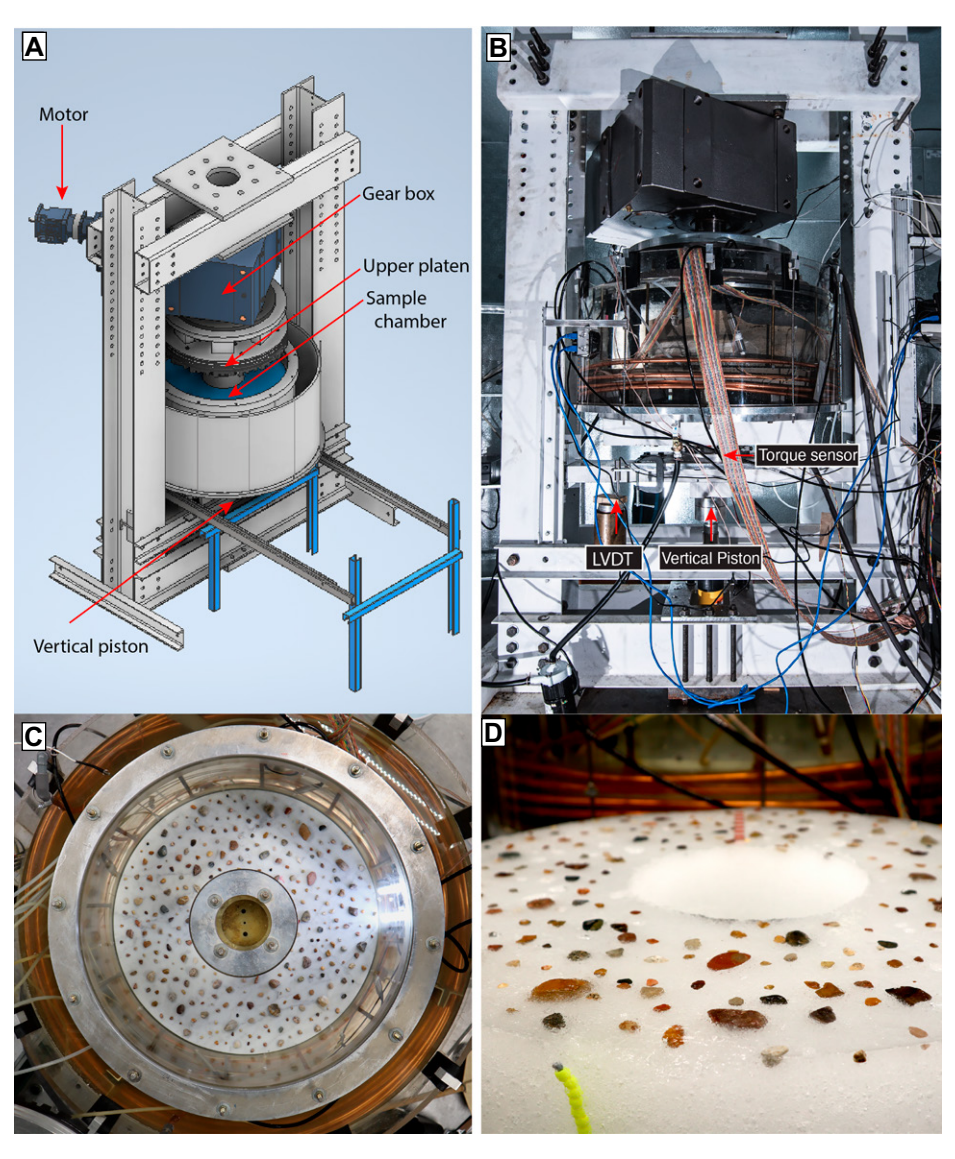


Figure 3. (A) Annotated schematic of the ring shear device used in these experiments. The ring shear is approximately 3 m tall. (B) Annotated image of the ring shear device used in these experiments. LVDT stands for linear variable differential transformer. (C) Image of debris placement atop the bed of the ring shear device prior to the experiment. The marble bed diameter is 60 cm. (D) The base of the ice ring flipped upside down following the experiment. The vast majority of the clasts are still located at the ice-bed interface, and there is minimal cavity formation in their lee.

was recorded via referenced photos (Fig. 3C; Fig. S2). These clasts were divided into three size categories: 25 large (20–28 mm diameter), 72 medium (12–20 mm), and 212 small (5–12 mm). Two experiments were conducted with all glaciological variables (e.g., slip speed, normal stress) held constant except the vertical melt rate, which was consistent within an experiment but varied between two experiments. The vertical melt rate is a dominant control on contact force between clasts and the bed and the resulting resistive shear stress due to debris-bed friction (Hallet, 1979, 1981). The low-stress experiment

(RS1) had an average vertical ice velocity of 560 mm/yr, compared to an average of 780 mm/yr for the high-stress experiment (RS2). The sliding speed for both experiments was 37.5 m/yr at a radial position that divided the area of the bed in half. The total ice displacement (81 cm for RS1; 71 cm for RS2) was less than the total circumference (~120 cm) of the ice ring to avoid significant overprinting of the striations. A torque sensor was outfitted on the base of the ring shear device to allow for continuous measurement of the shear stress exerted by the debris-laden ice ring slipping atop the rotationally fixed bed (for a

more detailed description of the device, see Zoet et al., 2023).

# 3.2. Morphology Imaging and Normalization

To calculate the length of each individual striation, high-resolution pictures were taken, and an orthomosaic georeferenced image of the entire marble bed piece was made using the Metashape software package. This georeferenced image was imported into QGIS, and each individual striation length was manually mapped (Fig. 4). Each striation was then classified based on its morphology (i.e., type 1, 2, or 3). The striation lengths were then normalized by the maximum displacement for their radial position in the ring using a MATLAB script. Using the x-y position data from the QGIS mapping and dividing the striation length by the maximum displacement that could have occurred at that radial position (from the known measured displacement of the ice ring) produced the normalize length of each striation. If, for example, the striation length equaled the total rotation displacement of the ice ring, then its normalized length value would equal 1. This normalization allowed us to directly compare striations from the inner portion of the ring with those from the outer portion, where displacement was greater. This normalization also allowed us to estimate the percent of striations remaining (cumulative abundance) at any given normalized displacement for comparison with the drag signal recorded in the ring shear device. To estimate the percent of striations remaining, the cumulative striation abundance was tabulated at each normalized rotation displacement (ranging between 0 and 1). Simply put, immediately after the ring began spinning, all of the striations were actively being formed, but as spinning continued, an increasing number of clasts stopped forming striations. By knowing the radial positions and lengths of all striations, we could directly determine the displacement at which a loss of striation occurred. We then summed the total number of clasts forming striations that remained for every possible normalized displacement between 0 and 1 to determine if there was a correlation between the number of clasts forming striations and the measured drag and if a certain type of striation contributed more to the sustained drag response. The recorded drag was also divided by the abundance of striation at each normalized displacement to determine if the stress per clast was changing with displacement.

A Nanovea JR25 white-light interferometer and respective software were utilized to scan individual striations and collect three-dimensional (3-D) spatial data. Data collected from

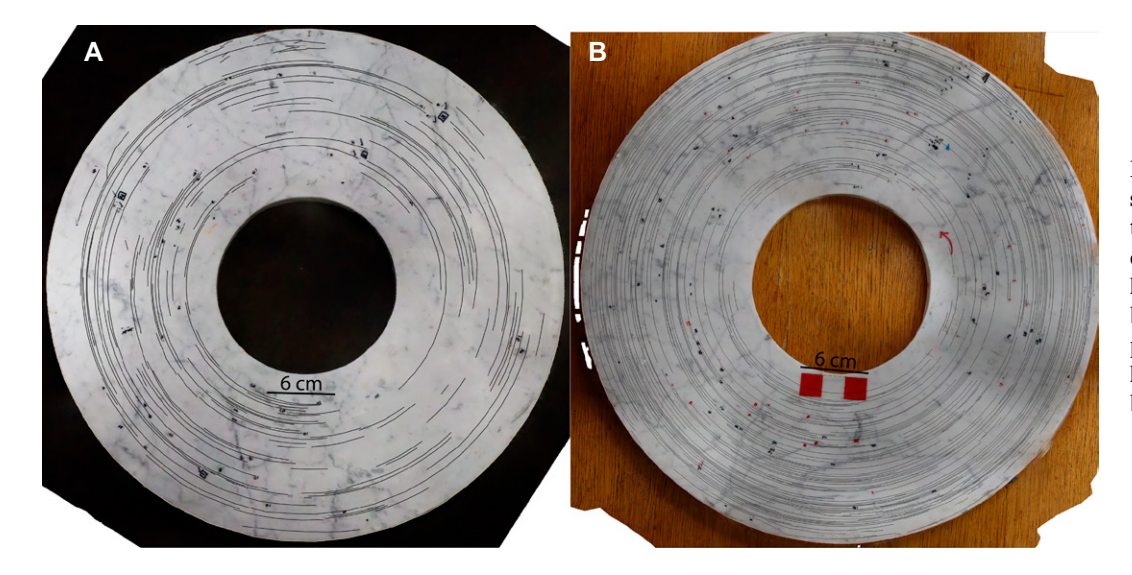


Figure 4. Marble bed with striations identified following the experiment. (A) Low-stress experiment with striations outlined in black on the marble bed piece. (B) High-stress experiment with striations outlined in black on the marble bed piece.

the Nanovea device were used to create depth profiles and 3-D models in the Professional 3D 7.4 software program. The profilometer was used to collect high-precision elevation information for a minimum of six striations per striation type for both stress conditions as well as many more lower-resolution profiles (catalog and data for all scans are provided in the Supplemental Material [see footnote 1]). For the high-resolution scans, the point spacing step values were set to  $10~\mu m$  for the x axis and  $15~\mu m$  for the y axis, and the vertical resolution was  $\sim 30~nm$ .

#### 3.3. Stress Inference

Using the drag record, it is possible to infer the maximum amount of clast rotation that would have been required to produce any observed change in the measured drag (following Iverson, 1991). The drag produced from an individual clast is related to the angle with which it indents the bed, as well as the frictional properties between the clast and bed. Just as we compared the change in distribution of striations with the change in drag, we also inferred the required adjustment in the clast angle from its original position needed to produce the drag record. The shear force,  $F_s$ , that a clast can provide by limiting frictional equilibrium can be expressed as

$$F_s = F_n \tan(\phi + \omega) \text{ for } (\phi + \omega) < 90^\circ,$$
 (1)

where  $\omega$  is the plowing angle of the clast,  $\varphi$  is the angle of sliding friction, and  $F_n$  is the normal force exerted on the clast by the ice flowing vertically toward the bed (Fig. 2; Iverson, 1990). In our experiments, the vertical flow

rate was largely held constant for each experiment, but at different values, so within a given experiment,  $F_n$  for clasts that remained in contact with the bed should not have varied significantly. The  $\phi$  also would not have changed within an experiment. Therefore, changes in  $F_s$  for a given clast throughout an experiment could arise from: (1) rotation of a clast while it remained in contact with the bed, indicating  $\omega$ would change; (2) a clast no longer ploughing but still in contact with the bed, indicating  $\varphi$ would remain constant, but ω would approach zero; or (3) a loss of contact with the bed, indicating both  $\omega$  and  $\varphi$  would approach zero. Assuming most clasts remained in contact with the bed, either 1 or 2 are viable explanations for a change in observed shear stress; however, if most clasts continued to form striations, then the changes in shear stress should have resulted from clast rotation.

For a subset of the striations, their cross-section profiles were extracted at regularly spaced increments along their long axis to estimate how the load, F, between the clast and bed changed as the striation grew, following equation 4.3 in Drewry (1986). First, the two-dimensional (2-D) cross section was used to estimate the crosssectional length over which the indenter was in contact with the bed, L. Assuming the indenter was round in shape, knowledge of L allowed for an estimate of the contact area. By virtue of the rock fracturing, it can be assumed the rock yield strength,  $\sigma_{v}$ , was met in the contact area ( $\sim 10$ MPa; Hansen et al., 2023), allowing for an estimate of the load, F, for each 2-D profile using the following expression,

$$F = \sigma_y \pi \left(\frac{L}{2}\right)^2. \tag{2}$$

#### 4. RESULTS

#### 4.1. Striation Abundance

In both the high- and low-stress experiments, we produced all three types of striations in addition to chatter marks (Fig. 5). In each of the experiments, we found that type 2 striations were initially the most abundant, followed by type 3 and finally type 1 and chatter marks (Table 1; Fig. 6). For the low-stress experiment ( $\bar{\tau} = 1.7 \text{ kPa}$ ),  $\sim 50\%$  percent of the clasts experienced enough normal and shear force to induce striations. For the high-stress experiment ( $\bar{\tau} = 4.2 \text{ kPa}$ ), that percentage rose to  $\sim 100\%$ , with some clasts producing multiple striations from multiple indenters. Following the completion of each experiment, nearly all clasts (>99%) were found to still be in contact with the bed (Fig. S1). There were minimal to no cavities found in the lee of clasts, indicating that minimal lodgment of the particles occurred on the bed, and so the clasts largely traveled the same distance as the ice. In both experiments past ~0.6 normalized displacement, no type 1 striations were observed (Fig. 6). Conversely, type 2, which started as the most abundant type of striation, diminished in number and became less abundant than type 3 striations. The type 3 striations were found to persist and become the most abundant type at large normalized displacements ( $>\sim 0.5$ ; Fig. 6).

## 4.2. Stress Observations

In each experiment, the drag was initially elevated and, with increased displacement, decayed to a near steady-state value after a normalized displacement of  $\sim 0.4$  (Figs. 7A

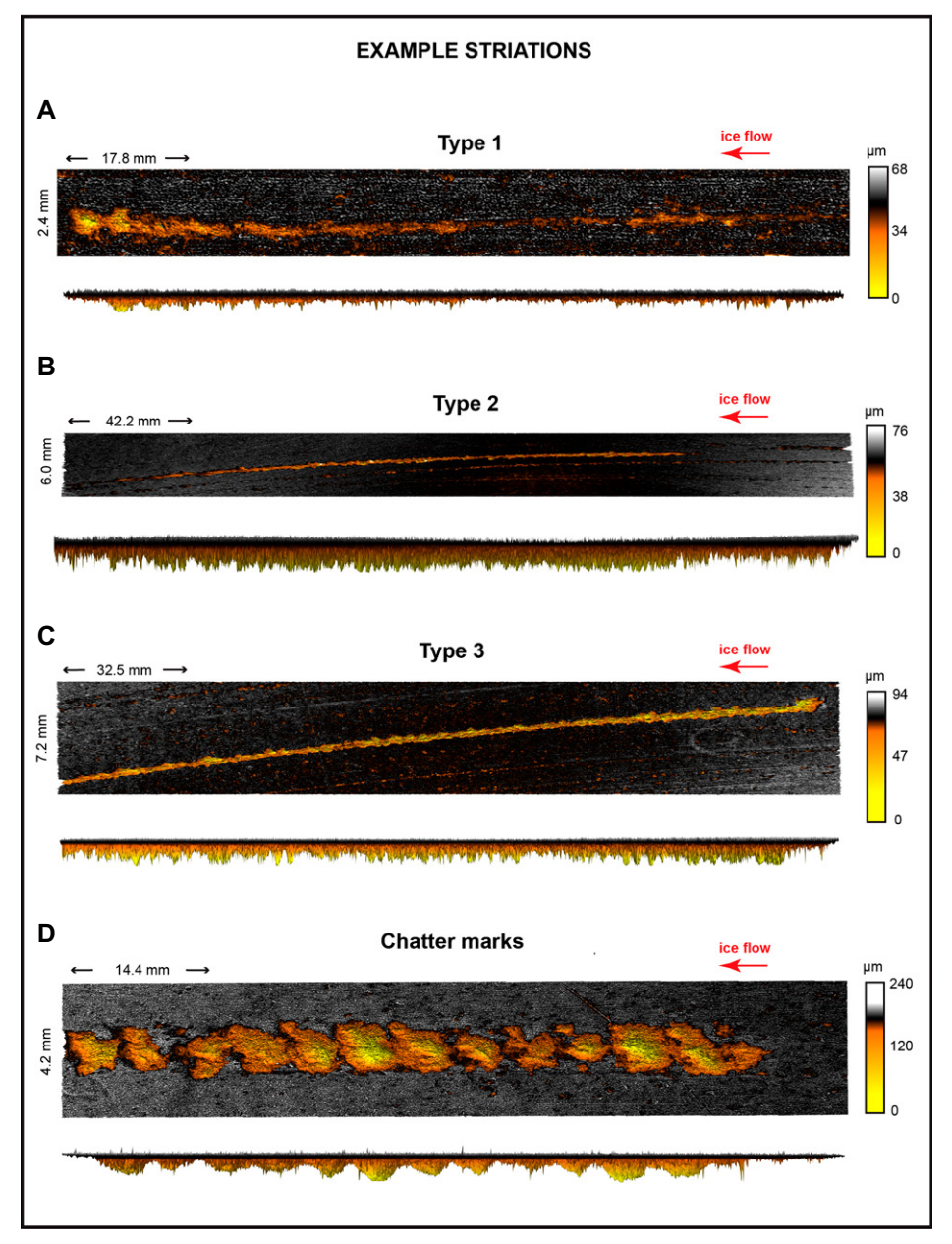


Figure 5. High-resolution scans of the various types of striations in both plan and profile view: (A) type 1 striation, (B) type 2 striation, (C) type 3 striation, and (D) chatter marks. In all panels, ice flow is indicated by the red arrows; 5% vertical amplification was added to the striation profiles to better visualize them.

TABLE 1. STRIATION COUNT

Туре	Low stress striation count $(n = 153)$	Low stress (%)	High stress striation count $(n = 460)$	High stress (%)	Low + high stress average (%)
Type 1	8	5.2	45	9.8	7.5
Type 2	62	40.5	160	34.8	37.6
Type 3	54	35.3	133	28.9	32.1
Chatter marks	1	0.6	23	5	2.8
Undetermined	28	18.3	99	21.5	19.9

and 7B). The normalized shear stress provided per clast (Fig. 7C) was constant and low for the initial portions of the experiment, but as the number of striations decreased (Figs. 7A and 7B), those clasts that were still indenting began to support an increased load (beginning at a normalized displacement of ~0.6; Fig. 7C). Another factor that will affect the contact force is the vertical melt rate, which did vary slightly about a mean in each experiment in a nonmonotonic fashion, and it did correlate to sudden changes in drag (see Fig. 7). However, the sudden changes in melt rate were not responsible for the long-term trends observed in the drag time series (Fig. 7).

Comparison of the changes in drag with the striation count revealed that both factors decreased with nearly the same form (Figs. 7A and 7B). For the high-stress experiment, the e-folding reduction distance (the distance over which the value reduces by a factor of e) was 0.11 (7.8 cm) for the drag and 0.12 (8.6 cm) for the striation count. For the low-stress experiment, the e-folding reduction distance was 0.134 (10.9 cm) for the drag and 0.135 (10.9 cm) for the striation count. In each experiment, the e-folding distances were nearly the same between the drag response and the striation count, with an average e-folding distance of  $\sim$ 10 cm for both experiments.

Using Equation 1, we estimated the rotation of the clasts necessary to give rise to the measured change in drag (Fig. 7), which was converted to shear force (here assuming all the change in measured drag was due to clast rotation). We found that only modest clast rotations were necessary to account for the observed reduction in drag:  $\sim 2.75^{\circ}$  for the high-stress experiment and  $\sim 1.75^{\circ}$  for the low-stress experiment (Fig. 8). However, this does not consider the changing number of clasts forming striations on the bed. We note that most of the change in drag occurred soon after displacement was initiated, indicating that most of the clast rotation occurred soon after displacement began.

Along the profiles of the striations, the load imparted by the indenter varied in accordance with the different types of striations (Fig. 9; Fig. S3). For the type 1 striation, the load was low and then increased with distance, and for type 3, the opposite was true. For type 2, the load was relatively constant throughout the striation formation. Additionally, there were some instances where sets of striations were crossing at angles to one another in the unidirectional flow field (Fig. 10). In these instances, the striations that were misaligned with the flow field tended to be wider in breadth than the average striation.

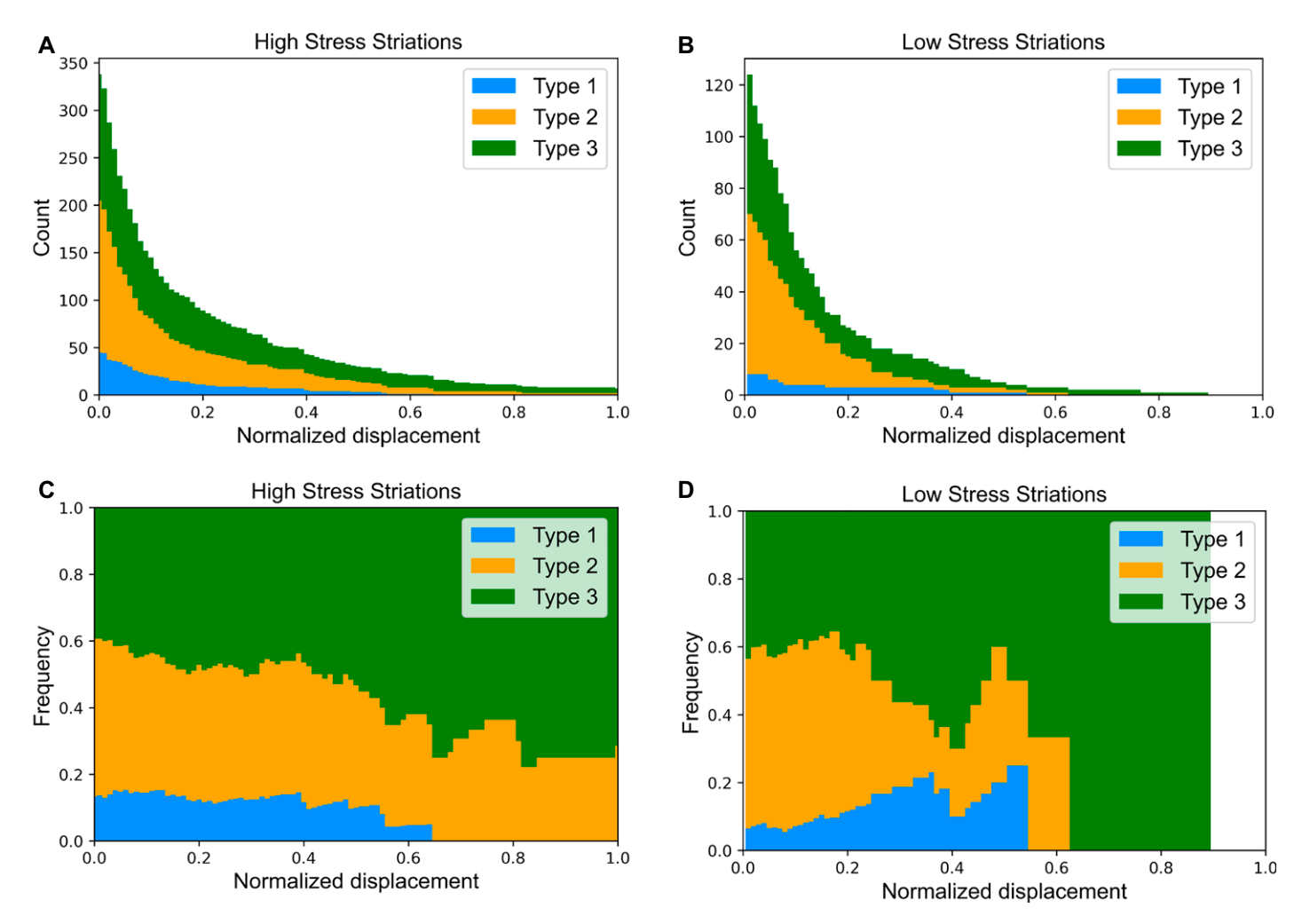


Figure 6. Plots of the striation abundance as a function of the normalized displacement (1 = full length). (A) Relative abundance of striation types 1, 2, and 3 for the high-stress experiment. Initially, type 2 is the most abundant. (B) Relative abundance of striation types 1, 2, and 3 for the low-stress experiment. Initially, type 2 is the most abundant. (C) Plot of striation abundance type for the high-stress experiment normalized by the total abundance at any given displacement. (D) Plot of striation abundance type for the low-stress experiment normalized by the total abundance at any given displacement.

## 5. DISCUSSION

The initial elevated drag was likely due to many clasts producing striations, but then as displacement increased, two mechanisms contributed to the observed stress reduction: (1) rotation of the clasts that were still forming striations and (2) cessation of striation by a subset of the clasts. In reality, these two mechanisms are closely linked, and it is the rotation of clasts that leads to the reduction in the number of clasts forming striations. Since the reduction of drag measured in the experiment closely resembled the reduction in clasts forming striations as a function of normalized distance (Figs. 7A and 7B), we favor mechanism 2 for providing a better direct explanation for the change in observed drag; however, changes in mechanism 2 are ultimately driven by changes in mechanism 1. Therefore, our find-

ings would seem to indicate that, when relatively large numbers of clasts forming striations are available, it is the abundance of clasts actively forming striations that to a first-order dictates the drag rather than changes in the angles of the clast indenters. Together, the relatively steady stress at large displacements (Fig. 7) and the small number of long striations (Fig. 6) indicate that steady-state drag resulted largely from those initial clasts that were optimally oriented to not plough themselves out. The relatively constant drag indicates that these processes, in the absence of a varying external factor, reached a sort of equilibrium that set the steady-state drag (Fig. 7). The striation depths were many times shallower than their widths (Fig. S3), suggesting that models for striation depth based on a hard penetrating cone (e.g., Drewry, 1986) are less valid than those based on a Hertzian indenter, as suggested by Thompson et al. (2020). Striations that were misaligned with the flow direction (Fig. 10), though few, provided an interesting observation that, at times, in addition to forward movement, clasts can experience appreciable lateral movement. In these instances, this mechanism may render it difficult to obtain a flow direction solely by measuring the long axis of the striation.

In agreement with field observations (Iverson, 1991), we found that type 2 striations initially dominated over types 1 and 3 (Fig. 6) for both the high- and low-stress experiments. Additionally, we found that shear stress in both experiments was initially high and then decayed with displacement. The distribution of striations showed that while type 2 striations initially dominated, many of them ploughed themselves out of existence, while type 3 striations were

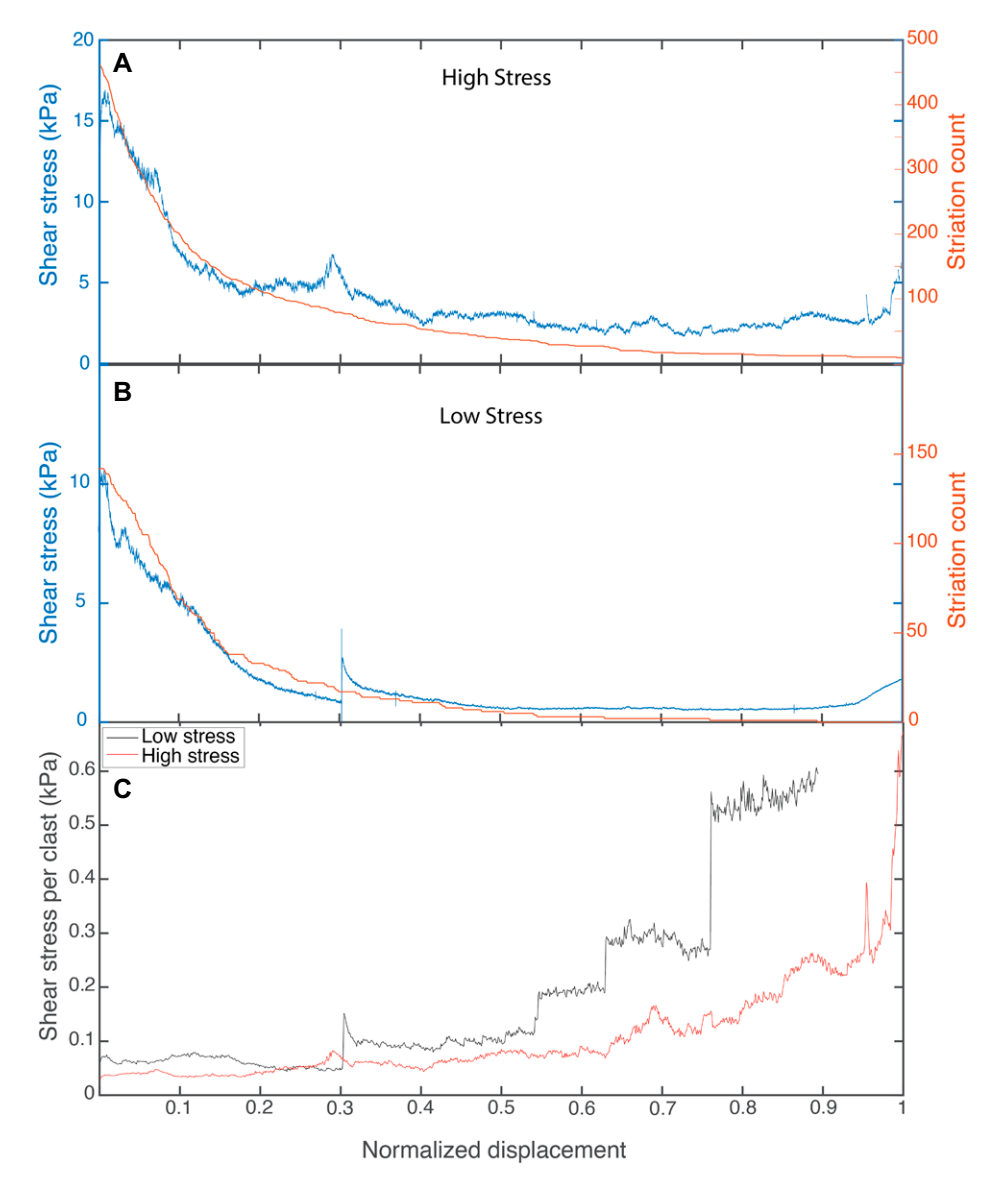


Figure 7. Comparison of shear stress record as a function of normalized displacement showing the change in the abundance of striations with normalized displacement. (A) Shear stress record for the high-stress experiments compared against the reduction in the total number of striations as a function of the normalized displacement. (B) Shear stress record for the low-stress experiments compared against the reduction in the total number of striations as a function of the normalized displacement. Note the similarity in the form of the curves and the *e*-folding distances (the distance over which the value reduces by a factor of *e*). (C) Normalized stress on a clast for both the high- and low-stress experiments. Initially, stress per clast is consistent and low, but then it begins to increase as the number of clasts dwindles, so stress is transferred to the remaining clasts.

often longer and became the dominant relative striation type at greater displacements (Fig. 7). A plausible hypothesis is that before sliding is initiated, many clasts are indented into the bed at a range of indenter angles, producing all three types of striations. Those clasts that are type 1, which are the minority in number, plough themselves into the bed, but after  $\sim 50\%$  of the displacement, they either find themselves

completely lodged, or they pop themselves out of their striations and essentially stop forming a striation (but still provide friction). Due to a lack of cavities observed in the lee of clasts following the experiment, it is unlikely the clasts lodged themselves completely. It appears that the smaller concentration of stress upon the indenter of type 3 relative to type 1 striations (from Eq. 1) due to the angle of the indenter leads the type 3

striations to reach a steady orientation whereby they can continue to form striations to greater lengths without completely rotating, removing, or lodging themselves. An interesting comparison is that, whereas Iverson (1991) found type 2 to be the most abundant in the field (as we also observed at low normalized displacements), type 3 came to dominate at higher normalized displacements in the experiment (Fig. 6), which was not observed in the field, indicating some aspect of the natural subglacial system is forcing the abrading environment to more closely resemble the conditions we had during the initial  $\sim 50\%$  of displacement rather than the conditions observed over the final  $\sim 50\%$  of displacement.

At the initiation of the experiment, the basal debris field was effectively "reset" due to the random clast placement, causing many of the clasts to become oriented such that striations were initially generated with slip. Then, with continued displacement, the striating clast numbers diminished as a large portion of the clasts ploughed or rotated themselves out of striations. Given the planar nature of the bed in our experiments, there were no natural obstructions to disrupt this process. In the natural world, a "resetting" process of the basal debris-laden ice may be expected to occur due to ice flow around the natural roughness of the basal terrain (which was absent in the experiment). A resetting of the basal debris field suggests that areas downstream of cavities or in the wake of obstacles where the clast orientations could be reset may favor greater clast-generated basal drag and abundance of striations (assuming other properties such as effective pressure and vertical ice flow rates are the same) by simply allowing more clasts to intercept the bed with a range of indenter angles. There is no reason to believe that the resetting process in the field requires a greater distance than that in the laboratory, where the e-folding distance was  $\sim$ 10 cm. Therefore, beds that have sufficient roughness elements at the length scales of 10 cm or shorter should be capable of resetting the basal debris field before it reaches the lowered steady-state drag, in theory giving rise to clast-induced drag that is elevated above the steady-state values and a dominance of type 2 striations.

The fact that Iverson (1991) found that type 2 striations dominate in the field for a region adjacent to Saskatchewan Glacier (Canada) would suggest that at least some natural glacier beds have sufficient roughness elements near  $\sim \! 10$  cm wavelengths for resetting. In fact, bed roughness observations have shown abundant spectral power below 10 cm for a range of glacier beds (Hubbard and Hubbard, 1998; Hubbard et al., 2000; Woodard et al., 2021, 2023), and Woodard et al. (2021) showed that roughness power was present in wavelengths below 10 cm for

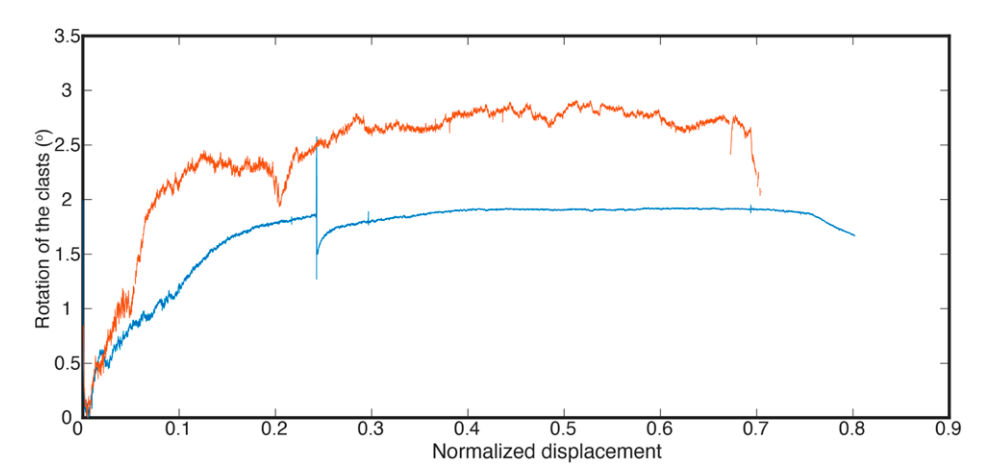


Figure 8. Amount of clast rotation that is needed to account for the observed change in drag plotted as a function of the normalized displacement for both the high-stress (orange) and low-stress (blue) experiments.

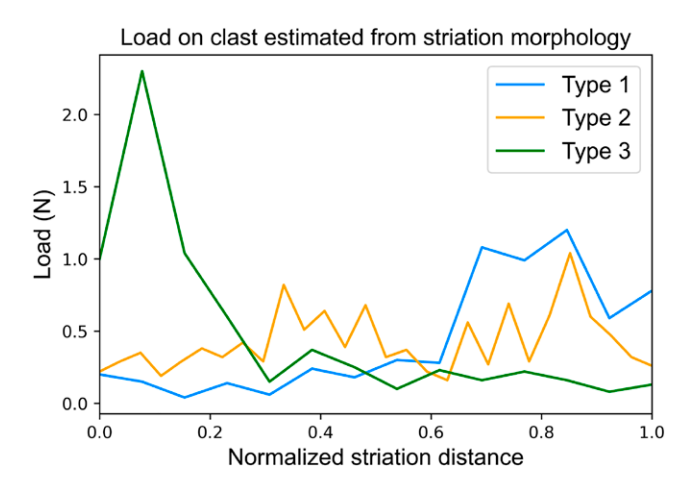


Figure 9. Load imparted on the bed by a clast as a function of the normalized striation distance. Load on the type 1 striation clast starts low and increases as the striation extends, opposite of the trend of type 3 striation clasts. Type 2 striation typically has a load that is relatively consistent throughout the length of the striation.



Figure 10. Striations that are not parallel to each other. The striation that is shown in black is aligned with the ice flow (which is radial), whereas the striation that is shown in blue is at an angle to the flow direction. The scale of the image is 8 cm from left to right.

Castleguard Glacier, which is immediately adjacent to Saskatchewan Glacier. Elevated roughness power below 10 cm should cause a nearly continuous resetting of the basal debris to keep clast-induced drag and basal abrasion rates elevated, which would effectively smooth the beds. However, the act of quarrying to continually roughen the bed could cause the tools of abrasion to become more effective by allowing more resetting of the basal debris field, suggesting the beds subject to elevated quarrying may also be subject to elevated rates of abrasion.

## 6. CONCLUSION

Glacial striations are produced in abundance at the beds of glaciers. We simulated their production in a laboratory device and found that between 50% and 100% of the clasts entrained in the basal ice initially produced striations, with the percentage depending on vertical ice velocity. As displacement continued, fewer and fewer clasts continued to abrade the bed, and near the end of the experiment, only a small percentage were still actively abrading. Along with this reduction in the number of abrading clasts, there was a similar reduction in the drag generated by the clasts, suggesting a relationship between the number of abrading clasts and the total resistive drag they can generate. The striations produced initially were dominated by type 2 striations, similar to field observations, but as displacement continued, the relative abundance of type 2 striations decreased, and type 3 striations became the dominant type. This dominance of type 3 striations at greater displacements likely stemmed from an indenter angle that allowed clasts to advance while still forming a striation without generating such large stress concentrations that they lodged themselves or popped out of the striation. We hypothesize that the abundance of type 2 striations initially in the experiment and their dominance in the field indicate that roughness in natural glacier beds allows the basal debris to "reset" itself when it encounters bed obstacles. This resetting may promote greater striations and larger numbers of type 2 striations on the down-ice side of obstacles (once clear of the pressure shadow effect on vertical flow rates). This would indicate that abrasion rates may be elevated in areas where the bed has been roughened, potentially from active quarrying. At a minimum, this investigation indicated that there is merit in understanding the distribution of striation population types that can be found in the field, especially in relation to bed obstacles, as they may serve as indicators of the basal dynamics and help to provide context for the importance of basal debris in providing drag for glacial slip. A study detailing the relative abundance of striations in and around obstacles could provide a means to spatially estimate variations in debris bed friction. (Note: We have placed many hundreds of high-resolution striation elevation profiles in the repository [http://digital.library.wisc .edu/1793/84816] as well as in the Supplemental Material [see footnote 1], so that they may be used as a baseline for interpreting glacial striations in the field.)

## ACKNOWLEDGMENTS

This project was supported by National Science Foundation grant EAR 2017185 awarded to L.K. Zoet. We would like to thank Chelsea Volpano for help constructing the orthomosaic photos and Danial Zuckerman for helping to digitize the striation measurements. We would like to thank Lauren Miller and one anonymous reviewer for suggestions that greatly improved the quality of the manuscript.

#### REFERENCES CITED

- Benn, D., and Evans, D.J., 2014, Glaciers and Glaciation: London, Routledge, 816 p., https://doi.org/10.4324 /9780203785010.
- Chamberlin, T.C., 1888, The rock scourings of the great ice invasions: U.S. Geological Survey 7th Annual Report, p. 155–248.
- Cohen, D., Iverson, N.R., Hooyer, T.S., Fischer, U.H., Jackson, M., and Moore, P.L., 2005, Debris-bed friction of hard-bedded glaciers: Journal of Geophysical Research: Earth Surface, v. 110, no. F2, F02007, https://doi.org/10.1029/2004IF000228.
- Drewry, D.J., 1986, Glacial Geologic Processes: Baltimore, Maryland, Edward Arnold, 276 p.
- Engelder, J.T., and Scholz, C.H., 1976, The role of asperity indentation and ploughing in rock friction—II: Influence of relative hardness and normal load: International Journal of Rock Mechanics and Mining Sciences & Geomechanics Abstracts, v. 13, no. 5, p. 155–163, https://doi.org/10.1016/0148-9062(76)90820-2.
- Gustafson, R.J., Hansen, D.J., and Folen, D.A., 1977, Finite Element Method Package: St. Paul, Minnesota, University of Minnesota, 87 p.
- Hallet, B., 1979, A theoretical model of glacial abrasion: Journal of Glaciology, v. 23, no. 89, p. 39–50, https://doi.org/10.3189/S0022143000029725.
- Hallet, B., 1981, Glacial abrasion and sliding: Their dependence on the debris concentration in basal ice: Annals of Glaciology, v. 2, p. 23–28, https://doi.org/10.3189/172756481794352487.

- Hallet, B., 1996, Glacial quarrying: A simple theoretical model: Annals of Glaciology, v. 22, p. 1–8, https://doi.org/10.3189/1996AoG22-1-1-8.
- Hansen, D.D., and Zoet, L.K., 2019, Experimental constraints on subglacial rock friction: Annals of Glaciology, v. 60, no. 80, p. 37–48, https://doi.org/10.1017/aog.2019.47.
- Hansen, D.D., Brooks, J.P., Zoet, L.K., Stevens, N.T., Smith, L., Bate, C.E., and Jahnke, B.J., 2023, A power-based abrasion law for use in landscape evolution models: Geology, v. 51, p. 273–277, https://doi.org/10.1130 //G50673.1
- Hubbard, B., and Hubbard, A., 1998, Bedrock surface roughness and the distribution of subglacially precipitated carbonate deposits: Implications for formation at Glacier de Tsanfleuron, Switzerland: Earth Surface Processes and Landforms, v. 23, no. 3, p. 261–270, https://doi.org/10.1002/(SICI)1096-9837(199803)23:3%3C261::AID -ESP848%3E3.0.CO;2-5.
- Hubbard, B., Siegert, M.J., and McCarroll, D., 2000, Spectral roughness of glaciated bedrock geomorphic surfaces: Implications for glacier sliding: Journal of Geophysical Research: Solid Earth, v. 105, no. B9, p. 21,295– 21,303, https://doi.org/10.1029/2000JB900162.
- Iverson, N.R., 1990, Laboratory simulations of glacial abrasion: Comparison with theory: Journal of Glaciology, v. 36, no. 124, p. 304–314, https://doi.org/10.3189/002214390793701264.
- Iverson, N.R., 1991, Morphology of glacial striae: Implications for abrasion of glacier beds and fault surfaces: Geological Society of America Bulletin, v. 103, p. 1308–1316, https://doi.org/10.1130/0016-7606(1991)103
- Iverson, N.R., 2012, A theory of glacial quarrying for landscape evolution models: Geology, v. 40, p. 679–682, https://doi.org/10.1130/G33079.1.
- Iverson, N.R., Cohen, D., Hooyer, T.S., Fischer, U.H., Jackson, M., Moore, P.L., Lappegard, G., and Kohler, J., 2003, Effects of basal debris on glacier flow: Science, v. 301, no. 5629, p. 81–84, https://doi.org/10.1126/science.1083086.
- Iverson, N.R., Helanow, C., and Zoet, L.K., 2019, Debris-bed friction during glacier sliding with ice-bed separation: Annals of Glaciology, v. 60, no. 80, p. 30–36, https:// doi.org/10.1017/aog.2019.46.
- Mathews, W.H., 1979, Simulated glacial abrasion: Journal of Glaciology, v. 23, no. 89, p. 51–56, https://doi.org /10.3189/S0022143000029737.
- Scholz, C.H., 1987, Wear and gouge formation in brittle faulting: Geology, v. 15, p. 493–495, https://doi.org/10.1130/0091-7613(1987)15<493:WAGFIB>2.0.CO;2.
- Scholz, C.H., and Engelder, J.T., 1976, The role of asperity indentation and ploughing in rock friction—I: Asperity creep and stick-slip: International Journal of Rock Mechanics and Mining Sciences & Geomechanics Abstracts, v. 13, no. 5, p. 149–154, https://doi.org/10.1016 /0148-9062(76)90819-6.

- Shah, K.R., and Wong, T.F., 1997, Fracturing at contact surfaces subjected to normal and tangential loads: International Journal of Rock Mechanics and Mining Sciences, v. 34, no. 5, p. 727–739, https://doi.org/10.1016/S1365-1609/97)00007-7.
- Stevens, N.T., Zoet, L.K., Hansen, D.D., Alley, R.B., Roland, C.J., Schwans, E., and Shepherd, C.S., 2024, Icequake insights on transient glacier slip mechanics: Earth and Planetary Science Letters, v. 627, https://doi.org/10 .1016/j.epsl.2023.118513.
- Thompson, A.C., Iverson, N.R., and Zoet, L.K., 2020, Controls on subglacial rock friction: Experiments with debris in temperate ice: Journal of Geophysical Research: Earth Surface, v. 125, no. 10, https://doi.org/10.1029/2020JF005718.
- Woodard, J.B., Zoet, L.K., Iverson, N.R., and Helanow, C., 2019, Linking bedrock discontinuities to glacial quarrying: Annals of Glaciology, v. 60, no. 80, p. 66–72, https://doi.org/10.1017/aog.2019.36.
- Woodard, J.B., Zoet, L.K., Iverson, N.R., and Helanow, C., 2021, Variations in hard-bedded topography beneath glaciers: Journal of Geophysical Research: Earth Surface, v. 126, no. 9, https://doi.org/10.1029/2021JF006326.
- Woodard, J.B., Zoet, L.K., Iverson, N.R., and Helanow, C., 2023, Inferring forms of glacier slip laws from estimates of ice-bed separation during glacier slip: Journal of Glaciology, v. 69, no. 274, p. 324–332, https://doi.org/10.1017/jog.2022.63.
- Zoet, L.K., Anandakrishnan, S., Alley, R.B., Nyblade, A.A., and Wiens, D.A., 2012, Motion of an Antarctic glacier by repeated tidally modulated earthquakes: Nature Geoscience, v. 5, no. 9, p. 623–626, https://doi.org/10 .1038/ngeo1555.
- Zoet, L.K., Carpenter, B., Scuderi, M., Alley, R.B., Anandakrishnan, S., Marone, C., and Jackson, M., 2013, The effects of entrained debris on the basal sliding stability of a glacier: Journal of Geophysical Research: Earth Surface, v. 118, no. 2, p. 656–666, https://doi.org/10.1002/jgrf.20052.
- Zoet, L.K., Ikari, M.J., Alley, R.B., Marone, C., Anandakrishnan, S., Carpenter, B.M., and Scuderi, M.M., 2020, Application of constitutive friction laws to glacier seismicity: Geophysical Research Letters, v. 47, no. 21, https://doi.org/10.1029 /2020GL088964.
- Zoet, L.K., Sobol, P., Lord, N., and Hansen, D.D., 2023, A ring shear device to simulate cryosphere processes: The Review of Scientific Instruments, v. 94, no. 4, https:// doi.org/10.1063/5.0142933.

SCIENCE EDITOR: MIHAI DUCEA ASSOCIATE EDITOR: PETRU URDEA

MANUSCRIPT RECEIVED 21 SEPTEMBER 2023 REVISED MANUSCRIPT RECEIVED 19 DECEMBER 2023 MANUSCRIPT ACCEPTED 12 JANUARY 2024